^{3}He$(e,e'p)^2$H breakup process

E. van Meijgaard
TRIUMF, 4004 Wesbrook Mall, Vancouver, British Columbia, Canada V6T 2A3

J. A. Tjon
Institute for Theoretical Physics, Princetonplein 5, P.O. Box 80.006, 3508 TA Utrecht, The Netherlands
(Received 18 January 1990)

The coincidence cross section of the electron induced two-body breakup reaction ^{3}He$(e,e'p)d$ is studied at various kinematic configurations. Nucleonic final-state interactions are treated exactly by solving the Faddeev equations for the relevant scattering states. The essential kinematic parameter in analyzing the results for the various kinematic regions is the missing momentum of the struck nucleon. At missing momenta below 250 MeV/c the s-wave analysis gives an adequate description of the experimental data. At missing momenta beyond 350 MeV/c a pure s-wave analysis is not sufficient. Contributions from the d-state components in the trinucleon wave functions to the disconnected graphs are considered.

I. INTRODUCTION

This paper describes some applications of the theoretical analysis presented in Ref. 1, herein called paper I. Recent experimental studies at Saclay[2,3] and at the Nationaal Instituut voor Kernfysica en Hoge-Energiefysica (NIKHEF), Amsterdam[4,5] have provided detailed and interesting data for the electron induced two-body breakup reaction of ^{3}He. With the objective to investigate the role of nucleonic final-state interactions we have calculated the two-body breakup cross sections at these various experimental kinematic situations, thereby using the solutions of the Faddeev equations in order to construct the wave functions for the three-nucleon bound state and the half-off-shell $NNN \rightarrow Nd$ scattering state at the relevant center of mass energies.

In presenting our results we distinguish kinematic configurations with different values for the missing momentum $p_m = |\mathbf{p}_{N'} - \mathbf{Q}|$ [see Eq. (65) in I]. In Sec. II we discuss two-body breakup results taken at low missing momenta ($p_m < 250$ MeV/c). In addition to the theoretical descriptions of the various kinematic situations we have carried out a systematic survey of the kinematic phase space in order to examine the size of final-state effects relative to the simple PWIA description. In Secs. III and IV we present a detailed treatment of a kinematic configuration studied at NIKHEF.[5] The experimental data were taken at missing momenta between 200 MeV/c and 500 MeV/c. At missing momenta beyond 350 MeV/c the s-wave analysis breaks down. This is discussed in Sec. III. A natural way to proceed is, of course, to repeat the analysis with non-s-waves in the nucleon-nucleon interaction taken into account. In Sec. IV we carry out the two-body breakup analysis with d-state components added to the disconnected contributions. Finally, in Sec. V we present results for the various nuclear structure functions.

II. FINAL-STATE EFFECTS AT LOW MISSING MOMENTUM

If the kinematics of an $(e,e'p)$ experiment is such that the knocked out proton has a low missing momentum, we expect that at high momentum transfer the scattering process is dominated by the PWIA. An example of such a situation is shown in Fig. 1. The experimental data[2] are taken at $Q = 428$ MeV/c, $\omega = 100$ MeV, and $E_e = 530$ MeV. Our results are plotted together with the results obtained by Laget,[6] who calculated the cross section from the first few terms of a diagrammatic expansion of the full transition amplitude. Meson exchange currents are also included in his calculations. The relative proton-deuteron energy T_{pd} is 60 MeV, and ten partial waves are used to include FSI. From Fig. 1 we see that for small initial moment p_m the agreement with experiment is good. At larger momenta the calculated results are too high, indicating that the high-momentum components of the UPA-MT wave function contain too little correlation. The Reid soft-core results of Laget in the PWIA indeed show a steeper falloff. The importance of the contributions of the PWIA and FSI amplitudes can be very different depending on the kinematic configuration. The PWIA amplitude, completely dominant at low initial momentum of the probed nucleon, falls off rapidly with increasing missing momentum p_m. For the FSI amplitude, we find a much slower falloff as a function of the same momentum. Since it turns out that the PWIA amplitude and the real part of the FSI amplitude have opposite signs, the real part of the full amplitude, which results from a coherent sum of all diagrams in Fig. 10 of I is considerably reduced at larger missing momenta. Part of this cancellation is compensated by the imaginary part of the connected amplitude. However, the size of the imaginary part is generally smaller than the size of the real part of the connected amplitude. Con-

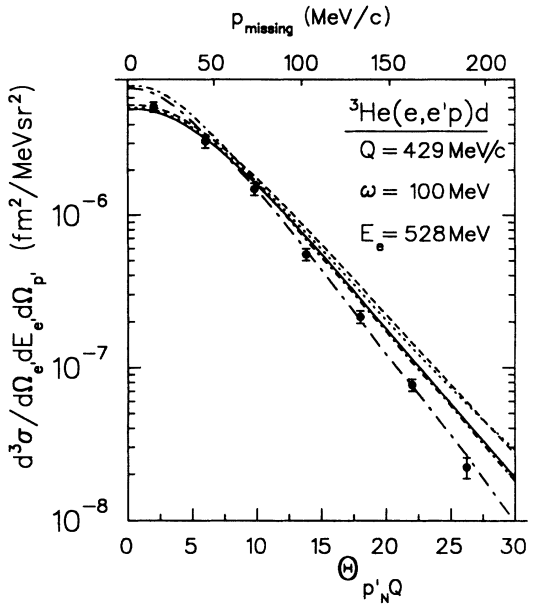

FIG. 1. PWIA dominated configuration studied at Saclay (Ref. 2). The solid and the dashed curve represent the results for the Born+FSI and the Born calculation. The dotted curve shows the result for the Born+rescattering connected diagrams (i.e., diagrams $a+b$ in Fig. 10 of I). The remaining curves are results from Laget (Ref. 6), representing a PWIA (short-dashed–dotted) and full (long-dashed–dotted) calculation, the latter including effects of meson-exchange currents.

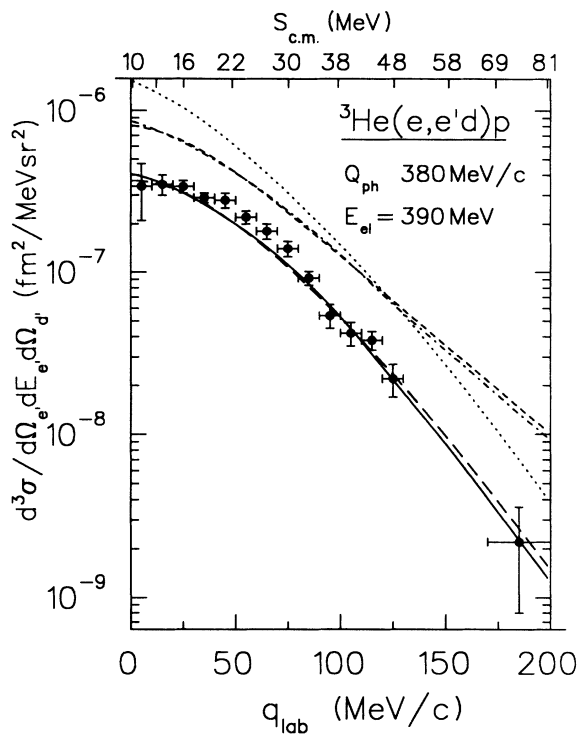

FIG. 2. Coincidence data (Ref. 4) taken at fixed momentum transfer in antiparallel kinematics. The short-dashed–dotted and solid curve represent, respectively, a Born and Born+FSI calculation with the local MT interaction. The short-dashed (Born) and long-dashed (Born+FSI) curve are obtained with the UPA separable expansion. The dotted curve shows the cross section calculated with the Born and the lowest-order connected diagrams, also determined with the UPA expansion.

sequently the addition of final-state effects gives rise to a decrease of the cross section in most kinematic situations.

Recently an interesting kinematic situation has been studied experimentally at NIKHEF, Amsterdam.[4] The results are shown in Fig. 2. This experiment is taken at antiparallel kinematics, i.e., $\hat{\mathbf{p}}'_N \cdot \hat{\mathbf{Q}} = -1$. This choice eliminates the contribution to the cross section from the nuclear structure functions W_S and W_I. The momentum transfer is fixed at 380 MeV/c, but the energy transfer varies from 10 MeV up till 80 MeV in the center of mass frame. The incoming electron energy is 390 MeV. In this kinematics, the pure PWIA result (not shown in the figure) predicts a cross section, which underestimates the experimental data by three orders of magnitude. This can be easily understood, realizing that in a direct nucleon knockout process at antiparallel kinematics the probed missing momenta are larger than the momentum transfer. Moreover, the dominant process in this kinematics is direct deuteron knockout (DDKO). Assuming this mechanism, the missing momentum corresponds to the initial momentum of the pair subsystem prior to the knockout, which is equal to the size of the recoil momentum of the outgoing nucleon. Indeed, the contributions from the disconnected diagrams already lead to the correct order of magnitude, but now the influence of FSI is much more pronounced than it is in the previously discussed kinematic configurations. Moreover, the reproduction of the experimental data is quite satisfactory. Both the UPA-MT and the local MT results are shown in Fig. 2. From this we see that the UPA result already gives a very accurate description in this kinematic situation. Following Laget, one possible approximation to the connected three-body amplitude is to keep only the lowest order connected diagrams or rescattering amplitudes. The calculated result is given by the dotted curve in Fig. 2. It is clear that the approximation is poor in this case of antiparallel kinematics and that it is necessary to determine the complete multiple scattering series.

Realizing that the deuteron momentum distribution inside ^{3}He is equal to the proton momentum distribution ρ_2 of ^{3}He, the Amsterdam group attempted to describe the breakup process as direct deuteron knockout, treating the deuteron as an elementary particle in the same way as is done with the nucleon. Instead of Eq. (65) of I, they factorized the cross section into ρ_2 times some phenomenological electron-deuteron cross section σ_{ed}. In doing so they just replaced the mass and the nucleon electromagnetic form factors in the expression for σ_{eN} [Eq. (3) of I] by the equivalent deuteron numbers. The result yields a remarkably good description of the data. However, such a treatment is expected to underestimate the disconnected contribution, since the overlap with the $^1S_0$-$^3I_1$ components of the trinucleon system is completely suppressed in such a calculation. To see how large this contribution

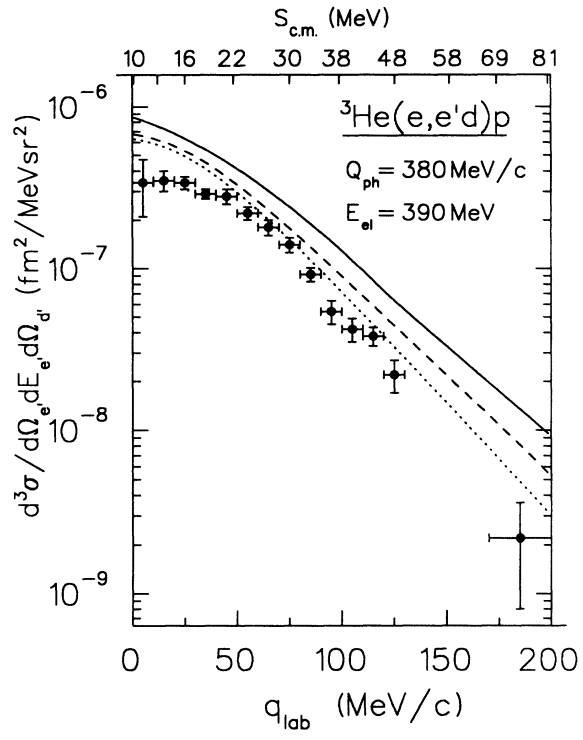

FIG. 3. Kinematics and data are the same as in Fig. 2. The solid curve shows the full UPA Born cross section. The dotted curve describes the phenomenological $\sigma_{ed}\rho_2(d)$ calculation. The dashed curve is a Born-type calculation, in which spin-isospin flips are neglected.

is, we have switched off the spin-isospin flip transitions in the disconnected amplitudes. The results are plotted in Fig. 3, together with the full Born result obtained with the UPA-MT potential. From this we see that indeed the $^1S_0$-$^3I_1$ amplitudes are also important and the agreement with the phenomenological electron-deuteron description can be considered fortuitous.

One of the crucial kinematic parameters in the analysis is the missing momentum. Although it is only well defined in a PWIA description, a similar parameter can be introduced to explain the DDKO contribution. In most experiments the missing momentum is varied indirectly with the purpose to extract the momentum distribution of ^{3}He from the measured cross section. However, such an analysis will yield rather unreliable information due to the unknown size of final-state effects. With the motivation to improve this situation we performed a more systematic study of the relative size of final-state effects as a function of the various kinematic variables. Since the momentum distribution is essentially a function of the missing momentum only, we found it instructive to fix this parameter at a number of values from 50 to 200 MeV. Figure 4 shows results as a function of the momentum transfer. The center of mass energy $s_{\text{c.m.}}$ is fixed at values 30, 60, and 90 MeV. In Fig. 5 we show the same results, but now as a function of the missing momentum at values for Q of 300, 400, and 500 MeV/c. All results shown in Figs. 4, 5, and 6 are calculated with the UPA-MT interaction, using nonrelativistic kinematics for the outgoing proton and deuteron. Use of relativistic kinematics will slightly affect the values along the horizontal axis. It is obvious that final-state effects play a more significant role at larger missing momentum. Furthermore, final-state effects are less important at higher momentum transfer or at higher center of mass energy. The angle $\cos\gamma_m = \hat{\mathbf{p}}_m \cdot \hat{\mathbf{Q}}$ is taken as the fourth kinematic variable to match the conditions of momentum-energy conservation. For each curve this angle roughly varies from antiparallel to parallel with respect to the three-momentum transfer. In Fig. 4 the point at the lowest Q values corresponds to $\gamma_m = 180°$, while the other end of each curve corresponds to $\gamma_m = 0°$.

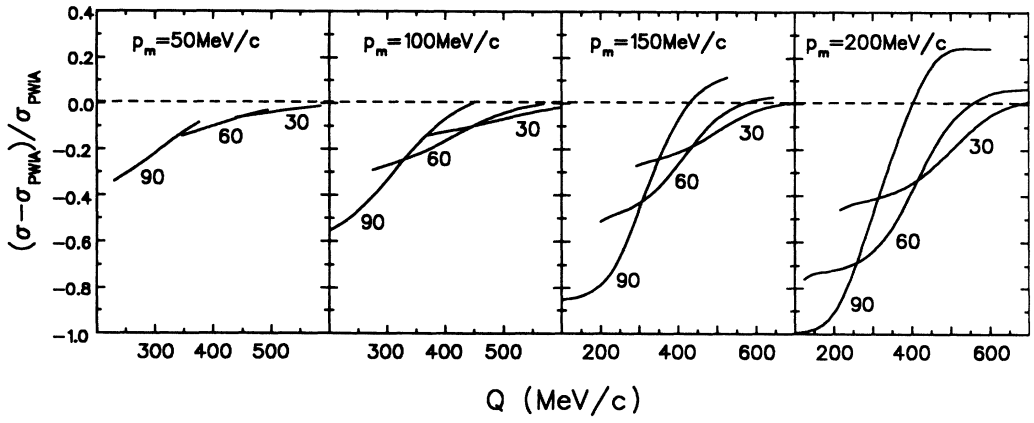

FIG. 4. Relative size of final-state effects versus momentum transfer at fixed missing momentum. The various curves are calculated at fixed center of mass energy $s_{\text{c.m.}} = 30$, 60, or 90 MeV.

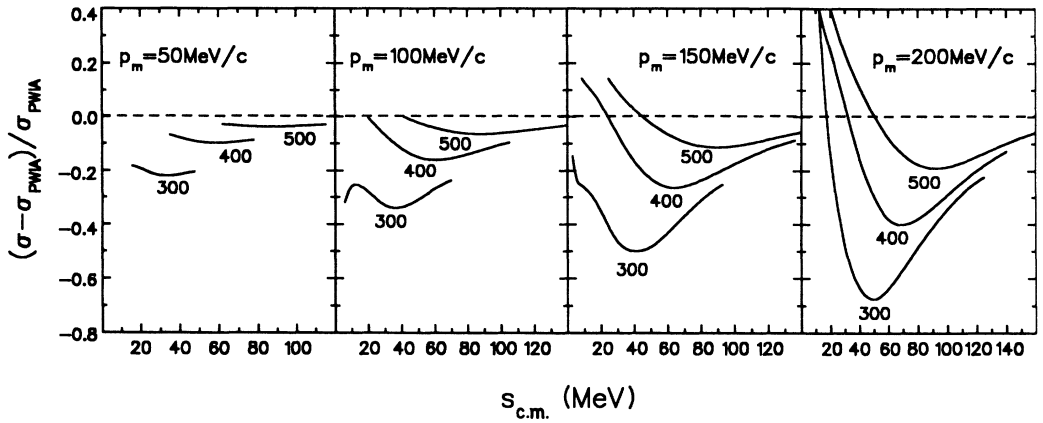

FIG. 5. Relative size of final-state effects versus center of mass energy at fixed missing momentum. The various curves are calculated at fixed momentum transfer $Q=300$, 400, or 500 MeV/c.

In Fig. 5 the situation is just opposite. Here the point at the largest $s_{c.m.}$ value corresponds to $\gamma_m=180°$, and the orientation gradually becomes parallel in going to lower values for $s_{c.m.}$. For all combinations of Q and $s_{c.m.}$ which are examined in these kinematic setups, the corresponding angle $\cos\gamma=\hat{\mathbf{p}}'_N\cdot\hat{\mathbf{Q}}$ of the outgoing nucleon will vary around the forward direction only. Consequently the DDKO process is suppressed and the renormalization of the PWIA cross section is entirely due to final-state effects.

The relative cross sections tend to have a minimum at the most off-parallel value of the angle γ, indicating that final-state effects are more important when the nuclear structure functions W_S and W_I contribute to the cross section. Moreover, final-state effects are least significant in parallel kinematics. To investigate this in more detail we fixed γ_m at 0°, 90°, and 180°, and varied Q and $s_{c.m.}$, simultaneously. The results are shown in Fig. 6. To get an idea of the variation of the center of mass energy $s_{c.m.}$, simply apply the quadratic relation $s_{c.m.}=E_d+(\frac{3}{2}\mathbf{p}_m+\mathbf{Q})^2/3M_N$. It is interesting to see that the parallel curves, labeled $\gamma_m=0°$, remain unaffected when the missing momentum is increased. The shape of the antiparallel curves, however, changes considerably, while the normal curves gradually move away from the parallel curves. We did not study the size of final-state effects at missing momenta beyond 200 MeV, since in this kinematic region d-state components of the wave function can no loger be ignored in the electromagnetic breakup analysis. This will be discussed in the next section.

III. FINAL-STATE EFFECTS AT HIGH MISSING MOMENTA

As shown in the previous section, the exact s-wave formalism is reasonably capable to give an adequate description of experimental data taken at low missing momenta. We now turn to the discussion of the experimental data in the region of high missing momenta. Recently, such a kinematic configuration has been investigated experimentally at NIKHEF, Amsterdam.[5] Two-body breakup data for ^{3}He were taken at constant energy-momentum

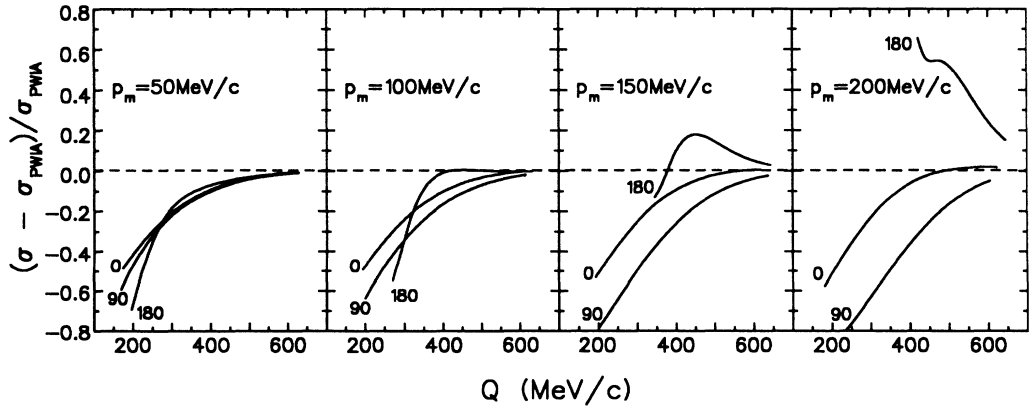

FIG. 6. Relative size of final-state effects versus momentum transfer at fixed missing momentum. The various curves are calculated at fixed angle $\gamma_m=0°$, 90°, or 180°.

transfer $\omega=113$ MeV, $Q=250$ MeV/c, and incoming electron energy $E_e=390$ MeV. The corresponding relative center of mass kinetic energy is about 93 MeV. In a PWIA-type analysis, variation of the photon-nucleon angle $\theta_{Qp_N'}$ from parallel to antiparallel implies that the nucleonic missing momentum is sampled from 200 MeV/c up to about 500 MeV/c. But in analogy with the previously discussed antiparallel kinematic experiment, the deuteron can also be regarded as the knocked out particle. In that case the corresponding missing momentum would vary from 440 MeV/c down to 260 MeV/c. For experimental reasons the deuteron has been detected rather than the proton in the high missing momentum region. This modification in measuring procedure corresponds to changing the reaction plane angle ϕ of Eq. (11) of I from 180° to 0°. In the calculation this affects the sign of the nuclear structure function W_I. The experimental data are shown in Fig. 7, together with the results obtained with the local s-wave MT potential. The UPA results are also plotted. At low missing nucleon momenta the analysis fairly well describes the experimental data. In this kinematic interval the Born term is purely determined by the PWIA contribution. The local analysis is slightly below the UPA results which agrees with the momentum distribution ρ_2 (see Fig. 11 of I).

However, at high missing nucleon momenta the situation changes considerably. The disconnected cross section, fully determined by the direct deuteron knockout process, overestimates the data by roughly one order of magnitude. Moreover, it shows a steep increase in approaching antiparallel kinematics in agreement with the momentum distribution, but in contrast with the behavior of the experimental points. Inclusion of final-state effects results in a dramatic reduction of the cross section, which now is below the experimental data by about one order of magnitude. On the level of transition amplitudes the Born amplitude is almost canceled by the real part of the connected amplitude. Moreover, the imaginary part of the connected amplitude is of the same order of magnitude as the real part of the full amplitude. In should be noted that the result is completely stable against any reasonable variation of the numerical integration parameters. Since the result is so sensitive for the inclusion of final-state effects one may ask what happens if we keep only the first rescattering diagrams in the connected amplitude. As expected a large deviation is found from the full result (see Fig. 7). It is clear that any truncation of the multiple scattering series leads to totally unreliable results in these types of kinematic configurations. Moreover, in view of the destructive interference occurring in this kinematic region a proper treatment of the non-s-wave components in the NN interaction has to be done before reaching any definite conclusions.

The above calculations are in apparent disagreement with Laget.[7] Already his Born description is considerably lower than we find. This is surprising, since in particular one might not expect that incorporating d-state components in the Born graph would decrease the cross section. This discrepancy is at least partially due to

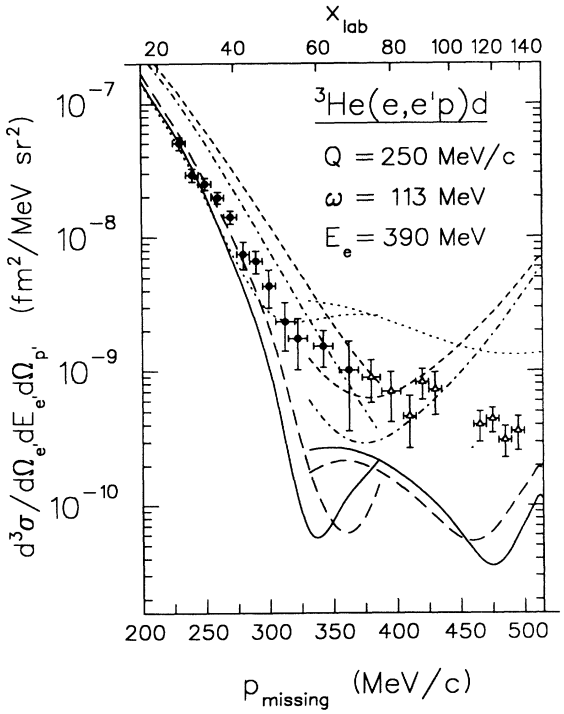

FIG. 7. Coincidence cross section taken at constant energy-momentum transfer at high missing momenta. The various curves are the same as in Fig. 2. Experimental data are taken at NIKHEF (Ref. 5).

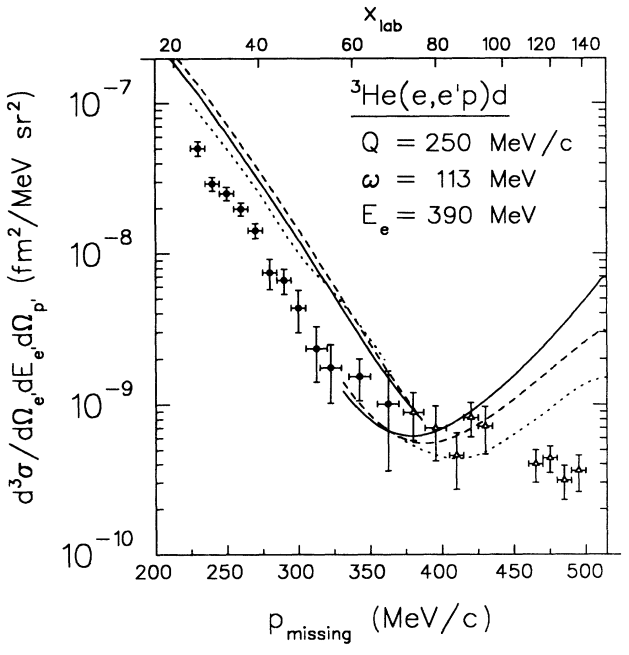

FIG. 8. Same kinematics as in Fig. 7. Solid line represents original Born calculation with UPA-MT interaction. Dashed line represents modified Born calculation with factorized trinucleon wave function (see text for explanation). The dotted curve is the Born-type result obtained by Laget using the Paris potential.

Laget's factorization approximation of the trinucleon wave function. To see how reasonable such an approximation is we have applied it also to our case. It consists of projecting out the $l=0$ component of the trinucleon wave function.

$$T_0(p,q)=\tfrac{1}{2}\int_{-1}^{1} d\cos\theta_{pq}\,\psi(p,q,\theta_{pq})$$

and approximating the wave function by

$$u_0(p)\chi_0(q)\rightarrow\tilde{\psi}_T(p,q)$$

with

$$u_0(p)=T_0(p,q=0)\ ,$$

$$\chi_0(q)=\frac{\int dp\,p^2u_0(p)T_0(p,q)}{\int dp\,p^2u_0^2(p)}\ .$$

The results for the electromagnetic breakup cross section are shown in Fig. 8. In the low missing momentum branch the factorization leads to fair results, however at high missing momenta this prescription is inadequate, resulting indeed in a decrease of the Born cross section by about a factor of 2.5 at the antiparallel point.

For this specific kinematic situation we performed two additional calculations. First we studied the dependence on the input parameters of the electromagnetic current. Figure 9 shows the various curves, where the result from Fig. 7 obtained with the relativistic current from Eq. (23) of I serves as a reference. Use of the current with the more convenient $\sigma_{\mu\nu}$ term leads to an almost indistinguishable result, while the nonrelativistic reduction of the current up to $\mathcal{O}(1/M_N^2)$ gives a reasonable result. Furthermore, note the flat behavior of the dotted line, which indicates that keeping the longitudinal component of the current instead of the charge component leads to entirely different predictions. We also mention the tendency of all curves to approach the same point at (anti)parallel kinematics, where the contribution from the structure functions W_S and W_I vanishes.

Finally we studied the convergence properties of the UPE separable expansion method for the electromagnetic two-body breakup cross section observable. The results are summarized in Fig. 10. The kinematics for which the curves are calculated corresponds to the $\phi=0$ branch of Fig. 7, and the experimental data are omitted. The results are self-explanatory and in accordance with the prior results on the bound state and scattering parameters. At low missing momenta the convergence properties are satisfactory. At high missing momenta the UPE calculations also converge, but not precisely to the local result. Probably, this difference, which persists if one calculates the cross sections for different combinations of the re-

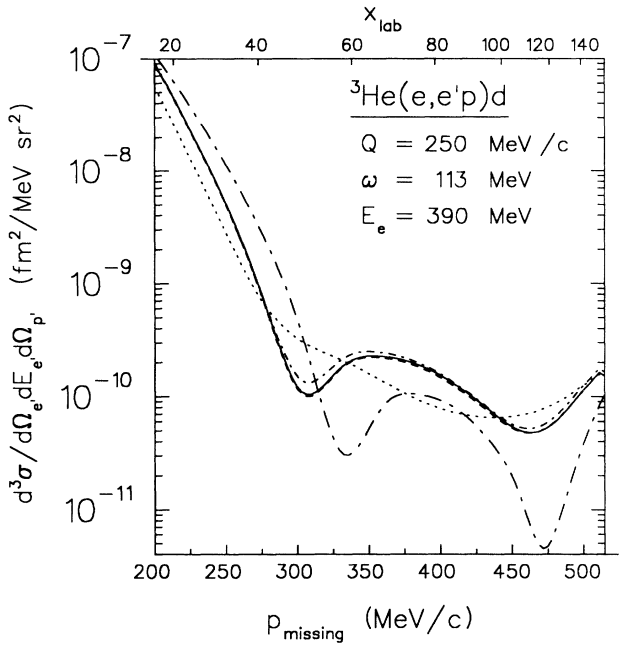

FIG. 9. Sensitivity study of various electromagnetic components in a kinematic situation equivalent to the high momentum region in Fig. 7. The solid line is the same as in Fig. 7. The dashed line is obtained with the current from Eq. (24) of I. The nonrelativistic reductions are shown by the long-dashed–dotted [$O(1)$] and short-dashed–dotted [$O(1/M_N^2)$] curves. Elimination of the charge components results in the dotted curve.

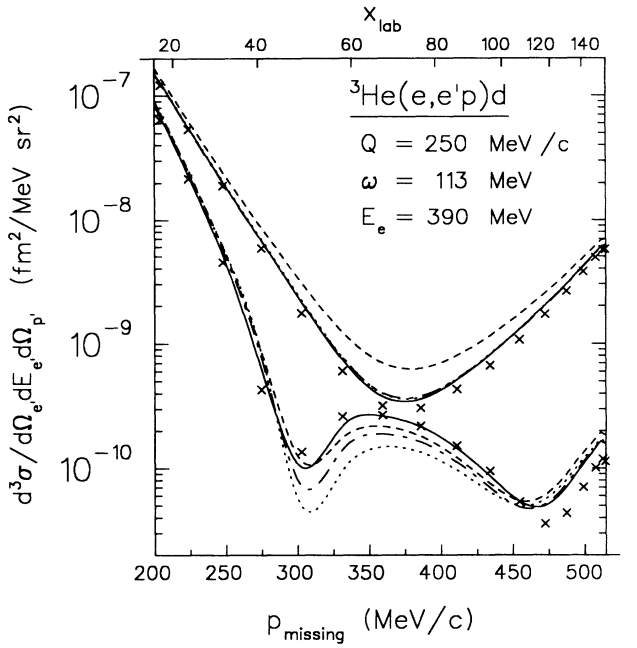

FIG. 10. Convergence properties of UPE in electromagnetic two-body breakup analysis. Kinematic situation is equivalent to the high missing momentum region in Fig. 7. The upper curves are Born results, while the lower curves include final-state effects. Crosses represent results from a calculation with the local MT interaction. The dashed curve corresponds to a UPA calculation. The long-dashed–dotted curve is also UPA, but obtained with the singlet parameter s set to 0 (see Appendix B of I). The dotted and solid curve are due to the (1111)-UPE and (2222)-UPE combinations.

tained UPE eigenvalues, must be ascribed to a slightly different behavior of the high momentum components in the scattering wave function. Somehow the electromagnetic observable is more sensitive to these components than the *Nd* scattering parameters, at least in the considered kinematic configuration.

IV. ANALYSIS WITH *d* WAVES IN THE DISCONNECTED GRAPHS

In the previous section we demonstrated that the *s*-wave analysis is not capable to describe the two-body breakup data at large missing momenta. It is expected that inclusion of non-*s*-waves components in the nucleon-nucleon interaction will improve the agreement with the data. To get some insight about their importance we studied their contribution to the Born graphs. Inclusion of final-state interactions in the connected graphs will be discussed in a forthcoming paper. For the two nucleon interaction we have taken the Reid soft-core (RSC) potential[8] acting in the $^3S_1$-$^3D_1$ and $^1S_0$ channels.

The electromagnetic breakup amplitude derived in the *s*-wave analysis of I can be straightforwardly generalized to an expression with higher partial waves in the *NN* interaction. We briefly discuss the structure of the amplitude and point out the differences with the description presented in Ref. 1. The nuclear current matrix element corresponding to the electromagnetic transition of the trinucleon bound state to the *Nd* outgoing scattering state is given by

$$A_\mu(d,j_d^z;\mathbf{q}_f,s_N^z;J_T^z)=\sqrt{3}\,{}^{(-)}_1\langle d j_d^z;\mathbf{q}_f s_N^z|J_{N_\mu}|\Psi_T J_T^z\rangle\ , \tag{1}$$

where the polarizations of the three-nucleon state, the deuteron, and the outgoing nucleon are denoted by J_T^z, j_d^z, and s_N^z, respectively. We assume that the nuclear current operator J_{N_μ} consists of one-body current contributions only, for which we take the on shell form given by Eq. (23) of I. Explicit expressions for the matrix elements of the one-nucleon current are summarized in Eq. (28) of I.

The nuclear structure tensor takes the form

$$\begin{aligned} W_{\mu\nu}=\tfrac{1}{2}\sum_{J_T^z}\sum_{j_d^z,s_N^z}&\delta(E_{p_N'}+E_{d'}-M_T-\omega)\\ &\times A_\mu^*(d,j_d^z;\mathbf{q}_f,s_N^z;J_T^z)\\ &\times A_\nu(d,j_d^z;\mathbf{q}_f,s_N^z;J_T^z)\ , \end{aligned} \tag{2}$$

where the energies are determined in the lab frame using relativistic kinematics. The various nuclear structure functions are derived from $W_{\mu\nu}$ according to Eqs. (14) and (15) of I. Similarly as in the *s*-wave analysis we evaluate the transition amplitude in the momentum representation. Using the complete set of three-nucleon momentum spin-isospin states from Eqs. (A5), we obtain

$$A_\mu(d,j_d^z;\mathbf{q}_f,s_N^z;J_T^z)=\sqrt{3}\sum_{n=1}^{3}\sum_{\beta_1}\int d\mathbf{p}_1 d\mathbf{q}_1\,{}^{(-)}_1\langle d,j_d^z;\mathbf{q}_f,s_N^z|\mathbf{p}_1\mathbf{q}_1\beta_1\rangle_1 R_\mu(n;\mathbf{p}_1,\mathbf{q}_1,\beta_1;J_T^z)\ , \tag{3}$$

where R_μ is given by

$$R_\mu(n;\mathbf{p}_1,\mathbf{q}_1,\beta_1;J_T^z)=\sum_{\beta_T}\int d\mathbf{p}_1'^{(n)} d\mathbf{q}_1'^{(n)}\,{}_1\langle \mathbf{p}_1\mathbf{q}_1\beta_1|j_\mu|\mathbf{p}_1'^{(n)}\mathbf{q}_1'^{(n)}\beta_T\rangle_1\,{}_1\langle \mathbf{p}_1'^{(n)}\mathbf{q}_1'^{(n)}\beta_T|\psi_T J_T^z\rangle\ . \tag{4}$$

The general form of the scattering wave function is, of course, much more elaborate than the pure *s*-wave form. However, in this work we only study the effect of *d*-wave admixture in the Born-type terms for which the outgoing scattering state is just the product of the deuteron state and a plane wave for the spectator particle. Explicit expressions for both the Born part of the scattering state and the wave function coefficients for the trinucleon bound state can be found in the Appendix. To include *s*-wave final-state effects we just take the result for the connected graphs from Eq. (80) of I. We only need to decouple the deuteron spin and the nucleon spin according to

$$\begin{aligned} A_\mu^{(\mathrm{FSI})}(d,j_d^z=s_d^z;\mathbf{q}_f s_N^z)&\\ =\sum_{S_f,S_f^z} A_\mu^{(\mathrm{FSI})}(d,\mathbf{q}_f,\beta_f)&\langle S_f S_f^z|s_d s_d^z s_N s_N^z\rangle\ . \end{aligned}$$

Momentum conservation at the electromagnetic vertex results in two delta functions for the three-momenta, which are removed by the integration of the variables $\mathbf{p}_1'^{(n)}$ and $\mathbf{q}_1'^{(n)}$. The momenta $\mathbf{p}_1^{(n)}$ and $\mathbf{q}_1^{(n)}$ are related to the remaining integration variables $\mathbf{p}_1$ and $\mathbf{q}_1$ according to Eq. (69) of I. The one-nucleon currents are evaluated for nucleon momenta $\mathbf{k}_n$ in the lab frame and its explicit spin structure is given by

$$j_\mu(\mathbf{k}_n,\boldsymbol{\sigma}_n,t_n^z)=S_\mu^0(\mathbf{k}_n,t_n^z)+i\mathbf{S}_\mu(\mathbf{k}_n,t_n^z)\cdot\boldsymbol{\sigma}_n\ . \tag{5}$$

Dependence on the isospin t_N^z is only present in the electromagnetic form factors. Like in the *s*-wave analysis we have to evaluate the matrix elements of the one-nucleon spin and isospin operators in three-nucleon Hilbert space. However, due to the spin-orbit coupling the various components of the spin operator interfere, and we prefer to take all amplitudes together. The evaluation becomes simpler if we write the one-nucleon current as

$$S_\mu=S_\mu^0+i(S_\mu^z\sigma^z+S_\mu^-\sigma^+ +S_\mu^+\sigma^-)\ , \tag{6}$$

where we have used the convenient definitions for $\sigma^\pm$ and $S_\mu^\pm$,

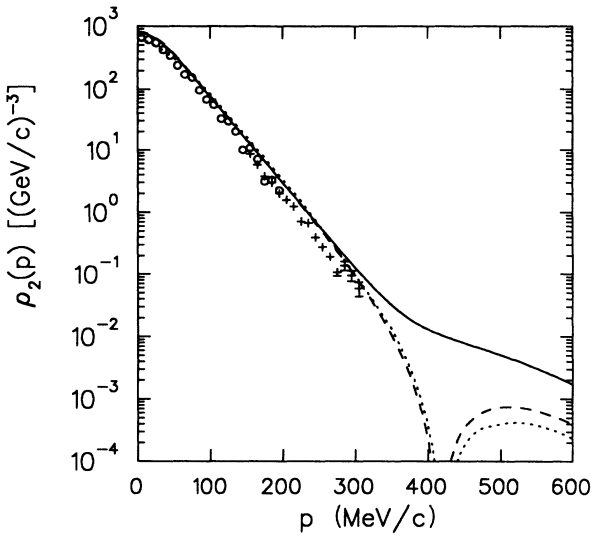

FIG. 11. Two-body momentum distribution ρ_2, calculated with the RSC interaction active in the $^1S_0$ and $^3S_1$-$^3D_1$ two-body channels. The solid line represents the full result. The dashed line corresponds to a calculation with the RSC potential confined to only the s-wave channels. For comparison the MT result is also plotted (dotted curve).

TABLE I. Faddeev components and their quantum numbers.

ν	$(l_p\ s_p)$	j_p	$(l_q\ s_q)$	j_q	$(t_p\ t_q)$	T
1	(0 0)	0	(0 $\frac{1}{2}$)	$\frac{1}{2}$	(1 $\frac{1}{2}$)	$\frac{1}{2}$
2	(0 1)	1	(0 $\frac{1}{2}$)	$\frac{1}{2}$	(0 $\frac{1}{2}$)	$\frac{1}{2}$
3	(2 1)	1	(0 $\frac{1}{2}$)	$\frac{1}{2}$	(0 $\frac{1}{2}$)	$\frac{1}{2}$
4	(0 1)	1	(2 $\frac{1}{2}$)	$\frac{3}{2}$	(0 $\frac{1}{2}$)	$\frac{1}{2}$
5	(2 1)	1	(2 $\frac{1}{2}$)	$\frac{3}{2}$	(0 $\frac{1}{2}$)	$\frac{1}{2}$

$$\sigma^+ = \begin{bmatrix} 0 & 1 \\ 0 & 0 \end{bmatrix} \text{ and } \sigma^- = \begin{bmatrix} 0 & 0 \\ 1 & 0 \end{bmatrix},$$

and

$$S_\mu^\pm = \tfrac{1}{2}(S_\mu^\parallel \pm i S_\mu^\perp) .$$

Explicit values for the matrix elements of σ^z are listed in Appendix D of I; the calculation of the matrix elements of $\sigma^\pm$ is, of course, completely equivalent. Once all the spin-isospin coefficients in three-nucleon space are known we can carry out the sum over the 16 spin-isospin states β_T in Eq. (4). It should be noted that this way of evaluating the spin stucture allows the direct calculations of nuclear polarization phenomena by simply isolating the

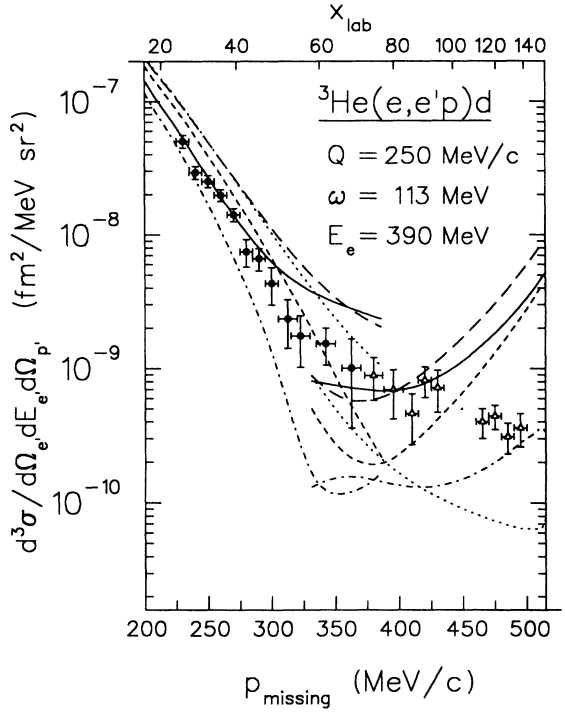

FIG. 12. Coincidence cross section at fixed energy-momentum transfer. Experimental data are from Ref. 5. The solid (long-dashed) curve corresponds to a Born+FSI (Born) calculation with d-wave NN components present in the disconnected graphs. The dotted curve represents the PWIA result. The short-dashed–dotted (short-dashed) curve shows the Born+FSI (Born) result obtained with the same interaction (RSC), but keeping only the $^1S_0$ and $^3S_1$ components of the two-body T matrix.

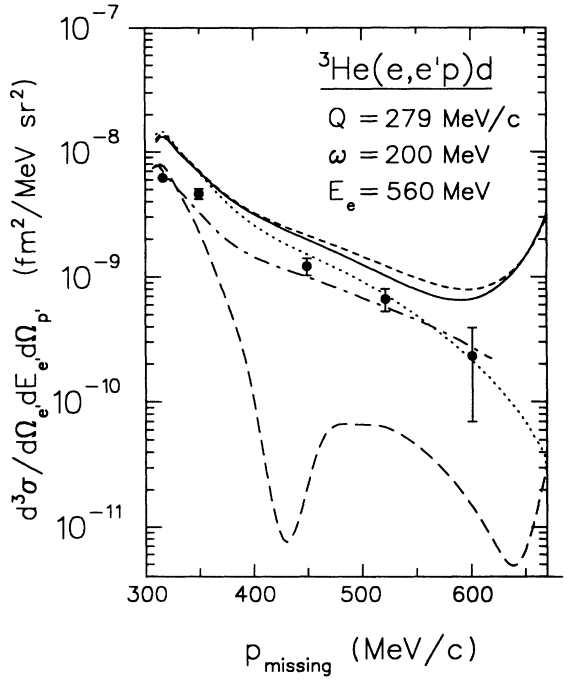

FIG. 13. PWIA dominated kinematics at high missing momenta. Data are from Saclay (Ref. 9). The solid, dashed, and dotted curves represent the Born+FSI, Born, and PWIA result, with d-wave NN components present in the bound state and disconnected final states. For comparison the pure s-wave result for a Born+FSI calculation is shown by the long-dashed curve. The long-dashed–dotted curve corresponds to a calculation by Laget (Ref. 7) including FSI and MEC effects.

various amplitudes which correspond to the initial and final polarization quantum numbers.

Let us turn to the results. The momentum distribution ρ_2 of ^{3}He obtained with the RSC-potential is displayed in Fig. 11. The figure clearly shows that the d-state component dominates the structure at missing momenta beyond 300 MeV/c. The result for the electromagnetic two-body breakup is presented in Fig. 12. The kinematics is the same as in Fig. 7. All results are calculated with the RSC potential as NN input. A result designated as s wave is obtained from the electromagnetic code after truncating the full T matrix in the coupled $^3S_1$-$^3D_1$ channels to the s-wave $^3S_1$ channel. It is obvious that inclusion of d waves in the disconnected graphs does not remedy the s-wave failure at high missing momenta. Addition of pure s-wave connected amplitudes only slightly improves the situation. But it is encouraging to see that the slope of this curve is in better agreement with the flat behavior of the experimental data at the highest missing momenta. We also examined the validity of the factorization assumption for the trinucleon wave function as employed by Laget[7] for simplifying reasons. This procedure essentially implies in this case that only the components $\nu=1$, 2, and 3 of the wave function are selected (see Table I). At high missing momenta this approximation suffers from the same flaw as already encountered in the pure s-wave analysis. The results are qualitatively the same as in Fig. 8 and we conclude that also for the five-channel trinucleon wave function the factorization assumption is not an adequate approximation to describe the coincidence two-body breakup data for missing deuteron momenta beyond 250 MeV/c in (near) antiparallel kinematics.

As a final example we present results for a rather different kinematics studied experimentally at Saclay.[9] The momentum-transfer parameters, $Q=279$ MeV/c and $\omega=200$ MeV are fixed in such a way that only the high missing momentum region is probed. Furthermore, the kinematic arrangement is such that direct nucleon knockout is the dominant process, except at angles close to antiparallel kinematics. The results are displayed in Fig. 13. Indeed, a PWIA calculation including d-state components gives an adequate reproduction of the data. Extending this result with the remaining set of diagrams improves the situation considerably, except at the highest missing momenta. This shortcoming is similar as encountered in the discussion of the Amsterdam kinematic situations.

V. NUCLEAR STRUCTURE FUNCTIONS

The contributions to the two-body breakup cross section come from the various nuclear structure functions W_j ($j=C,T,S,I$). In the special case of parallel kinematics the cross section is completely determined by W_C and W_T, which can be separated experimentally by the performance of two measurements with fixed momentum-energy transfer at different values of the electron energy E_0 and the scattering angle $\theta_{e'}$. For arbitrary kinematics the functions W_S and W_I also contribute to the cross section. The experimental separation of these additional structure functions requires a so-called out-of-plane measurement, in which the electron scattering plane and the hadronic scattering plane no longer coincide. Until now, such an experiment has not been done for the trinucleon system, but in view of possible future experiments it is interesting to see the structure of the various W functions. Therefore we have studied two kinematic situations, in which the laboratory angle $\gamma_{p'_N,Q}$ was varied from parallel to antiparallel. For the momentum transfer Q we took the values 259 MeV/c and 518 MeV/c. The energy transfer ω was chosen in such a way that the missing momentum p_m was approximately zero at parallel kinematics. The corresponding values for ω are 43 MeV and 148 MeV. The largest values of the missing momentum occur at antiparallel kinematics. For the considered kinematic situations these maximum values for the missing momenta are 345 MeV/c and 690 MeV/c, respectively. In view of these values an s-wave analysis is sufficiently accurate for the $Q=259$ MeV/c kinematics, whereas d waves must be included in the analysis of the $Q=518$ MeV/c kinematics. Of course, the latter can only be done for the disconnected contributions. The results for the nuclear structure functions are shown in Figs. 14 and 15. To calculate their contribution to the cross section one has to multiply the W functions with the appropriate electron-photon factor according to Eq. (13) of I. The pure s-wave result is calculated with the UPA-MT interaction, while the mixed $s+d$-wave result is obtained with the RSC potential. The figures clearly show that

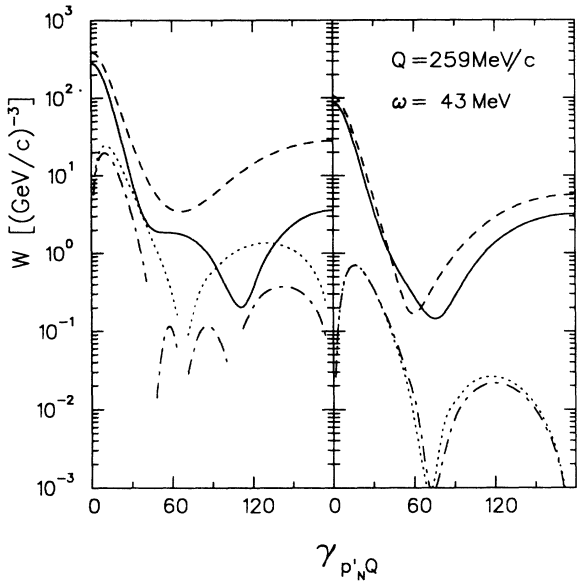

FIG. 14. Nuclear structure functions of the unpolarized ^{3}He($e,e'p$)d reaction calculated with the UPA-MT interaction. The left-hand part of the figure shows W_C and W_I. The dashed (dotted) curve and the solid (dashed-dotted) curve represent the Born and the Born+FSI results, respectively, for W_C(W_I). Similarly on the right-hand part, results are shown for W_T and W_S.

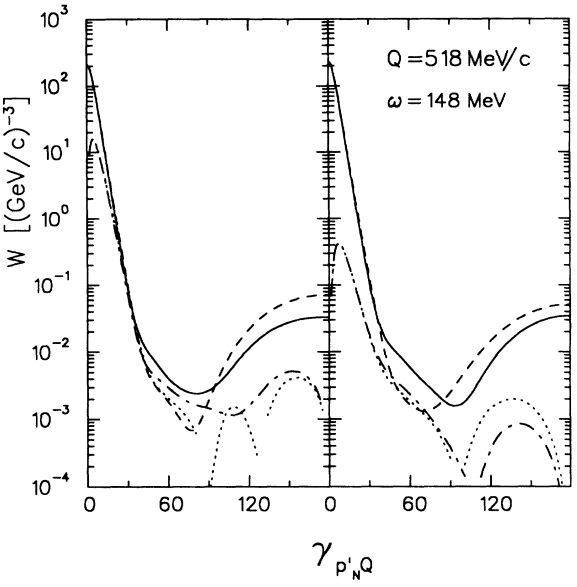

FIG. 15. Nuclear structure functions of the unpolarized ^{3}He($e,e'p$)d reaction calculated with the $s+d$-wave RSC potential. The meaning of the various curves is similar to Fig. 14.

W_C and W_T form the dominant contributions. However, W_I can be comparable in size with W_C and W_T at off-parallel kinematics. Note that W_I does not have a definite sign. W_S appears to be small relative to W_I. Furthermore, the renormalization due to final-state effects is evidently larger for W_C and W_I, both containing the charge component of the nuclear current, than it is for W_T and W_S, which are purely composed of the transverse parts of the nuclear current.

VI. SUMMARY AND CONCLUSIONS

In this paper we have presented a study of the effects of final-state interactions in the two-body electrodisintegration of ^{3}He. The required half-off-shell continuum trinucleon wave functions are calculated exactly by solving the Faddeev equations. Local s-wave spin-dependent NN potentials are used as input. Furthermore, the method of separable expansions of the two-nucleon T matrix are explored in the calculations of the electromagnetic matrix elements. In the kinematic regions considered the FSI are shown to play an important role and clearly cannot be neglected in the calculation of the amplitudes. Also in the longitudinal/transverse components of the structure functions separately, effects of FSI can be substantial,[10] which may have consequences in the discussion of possible medium modifications of the nucleon current. We have found that exact continuum wave functions must be used to account properly for the final-state interaction effects. In particular, approximations like the lowest order rescattering contributions in general fail to describe these effects in a correct way.

Two major conclusions can be drawn with respect to the studied kinematic configurations. At low missing momenta the renormalization of the nuclear structure functions due to final-state effects leads to satisfactory results. In particular the antiparallel kinematic setup studied at NIKHEF, Amsterdam, nicely illustrates how the experimental data are well reproduced by a purely nucleonic analysis with exact three-body dynamics. In contrast, at high missing momenta an analysis with NN interactions only present in the s-wave channel is totally incapable to describe the experimental data. The major reason is that the high momentum components in the nuclear wave function are probed in these types of experiments. The Born analysis considerably overestimates the experimental data at large missing momenta. Addition of only s-wave connected contributions only slightly improves the theoretical description. It is clear that d-wave components must be included in the connected amplitudes before any definite conclusions can be formulated about the ability of a theoretical description based on nonrelativistic nuclear dynamics and nucleonic degrees of freedom only to give a proper reproduction of exclusive two-body breakup data at intermediate values for the momentum-energy transfer. Such work is currently in progress.

ACKNOWLEDGMENTS

The authors thank Dr. P. de Witt Huberts for helpful discussions and for clarifying and detailed comments on the ($e,e'p$) experiments performed at the Nationaal Instituut voor Kernfysica en Hoge-Energiefysica (NIKHEF). We also thank Dr. P. Sauer for making his trinucleon bound state wave function available. Part of the numerical computations have been carried out on a Cyber 205. This was made possible by the Stichting Surf, the Netherlands.

APPENDIX: DEUTERON AND TRINUCLEON WAVE FUNCTIONS

The deuteron has total angular momentum $j_d=1$, spin $s_d=1$, and isospin $t_d=0$. Thus, the possible values for the orbital momentum are $l_d=0$ and $l_d=2$. Consequently, the deuteron state

$$|dj_d^z\rangle \tag{A1}$$

can be obtained from the residue of the two-body T matrix at the deuteron pole for the coupled $^3S_1$-$^3D_1$ channel, where the total angular momentum component j_d^z is a conserved quantum number with three possible values: $j_d^z=0,\pm1$.

In plane wave notation we obtain

$$|dj_d^z\rangle=\sum_{s_d^z}\int d\mathbf{p}|\mathbf{p}s_d s_d^z\rangle\langle\mathbf{p}s_d s_d^z|dj_d^z\rangle\ , \tag{A2}$$

where we have ignored the notation of the trivial isospin part ($t_d=t_d^z=0$). The coefficients of this projection are given by

$$\langle\mathbf{p}s_d s_d^z|j_d^z\rangle=\sum_{l_d=0,2}\phi_{l_d}(p)\sum_{s_d^z l_d^z}\langle l_d l_d^z s_d s_d^z|j_d j_d^z\rangle Y_{l_d}^{l_d^z}(\hat{\mathbf{p}})\ . \tag{A3}$$

In each coefficient the orbital component is fixed according to

$$l_d^z = j_d^z - s_d^z \ . \tag{A4}$$

Due to rotational invariance the radial components ϕ_{l_d} do not depend on l_d^z.

For the disconnected graphs of the two-body breakup process we combine the deuteron state with a plane wave for the outgoing nucleon. Projection on the basis states $|\mathbf{pq}\beta\rangle_1$ for the momenta, spin, and isospin of three particles,

$$|\mathbf{pq}\beta\rangle_1 = |\mathbf{pq};(s_p s_q)SS^z;(t_p t_q)TT^z\rangle_1 \ , \tag{A5}$$

yields the wave function coefficient

$${}_1\langle \mathbf{pq}\beta | dj_d^z; \mathbf{q}_f s_N^z t_N^z \rangle_1 = \delta_{t_p,t_d}\delta_{t_q,t_N}\delta_{s_p,s_d}\delta_{s_q,s_N}\delta(\mathbf{q}-\mathbf{q}_f)\langle TT^z | t_d t_d^z t_N t_N^z\rangle \sum_{s_d^z} \langle \mathbf{p} s_d s_d^z | dj_d^z\rangle \langle SS^z | s_d s_d^z s_N s_N^z\rangle \ . \tag{A6}$$

The trinucleon bound state is treated similarly. Conserved quantum numbers are the total angular momentum $J_T=\frac{1}{2}$, the z component $J_T^z=\pm\frac{1}{2}$, and the parity $\pi=-1$. The total spin can be either $S=\frac{1}{2}$ or $S=\frac{3}{2}$. Consequently, the orbital momentum can take the values $\mathcal{L}=0,1,2$. The spin S and spin component S_z are conserved in a pure s-wave analysis. If we adopt the following coupling scheme:

$$\left.\begin{aligned} l_p + \mathbf{s}_p &= \mathbf{j}_p \\ l_q + \mathbf{s}_q &= \mathbf{j}_q \end{aligned}\right\} \mathbf{j}_p + \mathbf{j}_q = \mathbf{J}_T \ , \tag{A7}$$

with

$$l_p + l_q = \mathcal{L}, \quad \mathbf{s}_p + \mathbf{s}_q = \mathbf{S} \ ,$$

it is immediately clear that we have in principle infinitely many possible values for the subsystem and spectator orbital momenta l_p and l_q. But it is natural to restrict the NN interaction for the spin-triplet state $s_p=1$ to the ${}^3S_1$-${}^3D_1$ channel, since we know that the deuteron is a major component of the trinucleon system. For the spin-singlet state $s_p=0$ we take again the ${}^1S_0$ partial wave. If we consider these partial waves, the Faddeev amplitude ψ_ν consists of five components ($\nu=1\cdots5$). Application of the $(j_p j_q)J$ coupling scheme from Eq. (A7) leads to the set of basis states

$$|p_i q_i \nu_i\rangle_i = |p_i q_i; [(l_{p_i} s_{p_i}) j_{p_i} (l_{q_i} s_{q_i}) j_{q_i}] JJ^z; t_{p_i} t_{q_i} TT^z\rangle_i \ . \tag{A8}$$

The relevant combinations are listed in Table I. In our calculations we used the set of Faddeev amplitudes generated by the Hannover group.[11] As NN interaction input they used the Reid soft-core (RSC) potential.[8]

To compose the three-body wave function we again start with the basis states from Eq. (A5). After transforming the plane wave states into angular momentum states according to

$$|\mathbf{pq}\rangle = \sum_{l_q m_q} \sum_{l_p m_p} Y_{l_p}^{*m_p}(\Omega_p) Y_{l_q}^{*m_q}(\Omega_q) |p l_p m_p; q l_q m_q\rangle \tag{A9}$$

the wave function components can be expressed as

$$\langle \psi_T J_T^z | \mathbf{pq}\beta_T\rangle_1 = \sum_{n=1}^{3}\sum_{\nu=1}^{5} \Gamma(\hat{\mathbf{p}}_n \hat{\mathbf{q}}_n; \nu; J_T^z; SS^z) \times \psi_\nu(p_n, q_n)\, {}_n\langle \beta_\nu | \beta_1\rangle_1 \ , \tag{A10}$$

where the coefficient Γ is shorthand for

$$\Gamma(\hat{\mathbf{p}}_n \hat{\mathbf{q}}_n; \nu; J_T^z; SS^z) = \sum_{\mathcal{L}\mathcal{L}^z} \sum_{l_p^z l_q^z} \langle (l_p s_p) j_p (l_q s_q) j_q J_T J_T^z | (l_p l_q)\mathcal{L}(s_p s_q) S J_T J_T^z\rangle \times \langle J_T J_T^z | \mathcal{L}\mathcal{L}^z S S^z\rangle \langle \mathcal{L}\mathcal{L}^z | l_p l_p^z l_q l_q^z\rangle Y_{l_p}^{*l_p^z}(\hat{\mathbf{p}}_n) Y_{l_q}^{*l_q^z}(\hat{\mathbf{q}}_n) \ , \tag{A11}$$

where the 9-j symbol is evaluated according to Edmonds.[12] In this expression the quantum numbers j_p, j_q, l_p, s_p, s_q are included in ν according to Table I. The coefficient ${}_n\langle \beta_\nu | \beta_T\rangle_1$ is the recoupling factor introduced in Appendix A of I. If we select only the pure s-state channels $\nu=1,2$, the results of Eq. (A10) should reduce to Eq. (53) of I. Indeed, the coefficient $\Gamma=1$ for $J_T=S$ and $J_T^z=S^z$, apart from a normalization factor $1/4\pi$, while it vanishes for the remaining combination of quantum numbers. The pure d-state channels $\nu=3,4$ only couple to the quartet state $S=\frac{3}{2}$. The relatively weak $\nu=5$ channel accounts for the mixing of the pure s-state and d-state channels. It furthermore contains the p-state component of the wave function, which is very small, about 0.08%.

The basis states in Eq. (A5) contain 16 orthonormal spin-isospin states. Together with the four spin doublet states with $S^z=J_T^z$, which are already present in the pure s-wave analysis, there are four $S=\frac{1}{2}$ states with $S^z=-J_T^z$. These latter states result from coupling to the $\nu=5$ channel and give rise to small contributions. Furthermore, the basis consists of spin quartet states, which have spin component $S^z=\pm\frac{1}{2},\pm\frac{3}{2}$. Each component occurs twice to account for the isospin subsystem number $t_p=0$ and $t_p=1$. In the quartet case the $t_p=1$ admixture is purely due to the exchange contributions in the wave function.

To check the correct numerical composition of the trinucleon wave function, we computed the normalization. Using the set of basis states in Eq. (A5), this opera-

tion becomes rather time consuming since a sixfold integral has to be performed together with a sum over n, ν, and β. Employing Gauss-Legendre quadratures with 16 points in the radial integrations [after mapping both radial meshes according to Eq. (79) of I with units $\sqrt{(\mathrm{MeV})}$ and $c_p=15$, $c_q=6.5$], eight points in the polar integrals, six points in the azimuthal integrals (ϕ_p:$\phi_q\rightarrow\phi_q+2\pi$;$\phi_q$:$0\rightarrow\pi$), the computed probabilities are $P(S=\frac{1}{2})=0.9089$ and $P(S=\frac{3}{2})=0.0911$. This result can be compared with the numbers listed in Table IV of Ref. 11, where the probabilities of the nontruncated wave function are found to be $P(\mathcal{L}=0)=0.9085$, $P(\mathcal{L}=1)=0.0$, and $P(\mathcal{L}=2)=0.0915$.

[1]E. van Meijgaard and J. A. Tjon, Phys. Rev. C **41**, 74 (1990) (preceding paper).
[2]E. Jans *et al.*, Phys. Rev. Lett. **49**, 974 (1982).
[3]E. Jans *et al.*, Nucl. Phys. **A475**, 687 (1987).
[4]P. H. M. Keizer, P. C. Dunn, J. W. A. den Herder, E. Jans, A. Kaarsgaarn, L. Lapikás, E. N. M. Quint, P. K. A. de Witt Huberts, H. Postma, and J. M. Laget, Phys. Lett. **157B**, 255 (1985).
[5]P. H. M. Keizer, J. F. J. van den Brand, J. W. A. den Herder, E. Jans, L. Lapikás, E. N. M. Quint, P. K. A. de Witt Huberts, and H. Postma, Phys. Lett. B **197**, 29 (1987).
[6]J. M. Laget, Phys. Lett. **151B**, 325 (1985), and private communication.
[7]J. M. Laget, Phys. Lett. B **199**, 493 (1987).
[8]R. V. Reid, Ann. Phys. (N.Y.) **50**, 411 (1968).
[9]C. Marchand *et al.*, Phys. Rev. Lett. **60**, 1703 (1988).
[10]E. van Meijgaard and J. A. Tjon, Phys. Rev. Lett. **61**, 1461 (1988).
[11]C. H. Hajduk and P. U. Sauer, Nucl. Phys. **A369**, 321 (1981).
[12]A. R. Edmonds, *Angular Momentum in Quantum Mechanics* (Princeton University Press, Princeton, NJ, 1957).